



CHORUS

This is the accepted manuscript made available via CHORUS. The article has been published as:

Role of descriptors in predicting the dissolution energy of embedded oxides and the bulk modulus of oxide-embedded iron

Keisuke Takahashi and Yuzuru Tanaka

Phys. Rev. B **95**, 014101 — Published 4 January 2017

DOI: [10.1103/PhysRevB.95.014101](https://doi.org/10.1103/PhysRevB.95.014101)

The Role of Descriptors in Predicting the Dissolution Energy of Embedded Oxides and the Bulk Modulus of Oxide-embedded Iron

Keisuke Takahashi*

*Center for Materials research by Information Integration (CMI²),
National Institute for Materials Science (NIMS),
1-2-1 Sengen, Tsukuba, Ibaraki 305-0047, Japan and
Graduate School of Engineering, Hokkaido University, N-13, W-8, Sapporo 060-8628, Japan*

Yuzuru Tanaka

Meme Media Laboratory, Hokkaido University, N-13, W-8, Sapporo 060-8628, Japan

(Dated: December 21, 2016)

Oxide-embedded bulk iron is investigated in terms of first principle calculations and data mining. 29 oxides are embedded into a vacancy site of iron where first principle calculations are performed and the resulting calculations are stored as a dataset. Prediction of the dissolution energy of oxides within iron and the bulk modulus of oxide-embedded iron is performed using machine learning. In particular, support vector machine (SVM) and linear regression (LR) are implemented where descriptors for determining the dissolution energy and bulk modulus are revealed. With trained SVM and LR, prediction of dissolution energy for different oxides in iron and the inverse problem – deriving corresponding descriptor variables from a desired bulk modulus – are achieved. The physical origin behind the chosen descriptors are also revealed where manipulating each individual descriptor within a multidimensional space allows for the prediction of the dissolution energy and bulk modulus. Thus, prediction of physical phenomena is, in principle, achievable if the appropriate descriptors are determined.

I. INTRODUCTION

Strengthening materials has been a fundamental interest of material scientists as the mechanical properties of the materials play crucial roles in a variety of areas, ranging from tool development to supporting advanced technologies. However, designing strengthened materials is challenging as the number of known structural materials is far outweighed by the unknown material possibilities. Development of mathematical algorithms associating with first principle calculations allows for the prediction of mechanical properties of materials, leading towards the rapid acquisition of material data [1–3]. With the large amounts of material data available, material design becomes achievable on the basis of trends and sequences in materials data upon the revelation of key descriptors [4–6]. Descriptors are defined as sets of variables determining material properties; therefore, descriptors can also be referred to as a material genome [1, 7]. In another words if descriptors for material properties are revealed, one can consider that prediction of material properties or material choice can, in principle, be achievable. However, the number of descriptors involved are often greater than 3 variables. Therefore, descriptors must be treated within a multi-dimensional space, making machine learning an effective tool for treating variables multidimensionally. Thus, combining first principle calculations and data science including machine learning has the potential to change how material science would be treated.

Oxide dispersion-strengthened (ODS) iron alloy is investigated as a prototype case for discovering key descriptors representing properties of ODS iron. The dispersion of metal oxides in a metal matrix is a technique used to increase the strength of metal for applications in extreme conditions such as high temperatures and high pressure as such alloys possess high thermal stability with good resistance against dislocation [8–10]. There are two important properties regarding ODS iron: the dissolution state of the oxide particles in the iron matrix and the bulk modulus of the oxide-embedded iron. The dissolution state of the oxide particles is important to ODS iron because the role of the oxides within the metal matrix is to halt dislocation due to the pinning effect. Within a high temperature environment, the prevention of thermal expansion is crucial where a high bulk modulus is considered be resistant against thermal expansion. Thus, the dissolution energy of oxides and bulk modulus are two key properties for designing ODS iron and descriptors representing the dissolution energy of oxides and bulk modulus are explored. In particular, the workflow shown in Figure 1 is proposed. First principle calculations are implemented to calculate oxide-embedded bulk iron and the calculated results are then stored as a database. Machine learning is utilized to find the descriptors responsible for the dissolution energy of oxides and the bulk modulus. Once the descriptors are determined, the machine can be trained using the corresponding database and, once trained, will be able to aid the design of ODS iron. In addition, the physical meaning behind the chosen descriptors are also investigated. Thus, the design of ODS iron is performed using first principle calculations and data mining.

* keisuke.takahashi@eng.hokudai.ac.jp

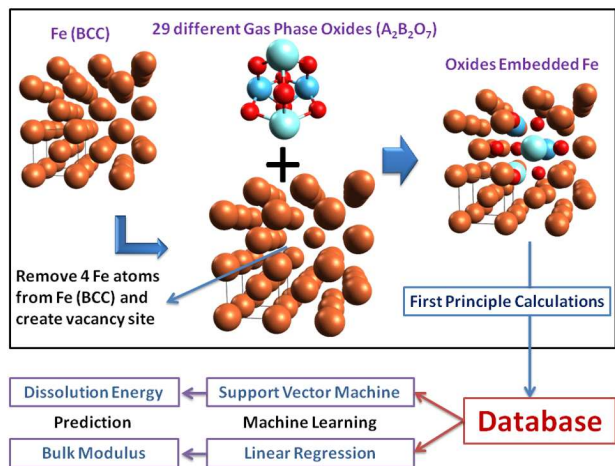


FIG. 1: A Proposed workflow of the atomic model construction, first principle calculations, database construction, machine learning, and prediction of the bulk modulus and dissolution energy of oxides. Atomic color code: orange– Fe, red– O, light and dark blue– element variables A and B.

II. DENSITY FUNCTIONAL THEORY AND MODEL

First principle calculations within grid based projector augmented wave (GPAW) method is implemented in order to calculate the material properties of oxide-embedded bulk iron [11]. The exchange correlation of Perdew–Burke–Ernzerhof (PBE) and spin polarization are applied [12]. The Γ point is used for calculating the gas phase oxide clusters while periodic boundary condition is applied for bulk calculations where $4 \times 4 \times 4$ special k points of the Brillouin zone sampling is used [13]. The dissolution energy (E_d) of oxide-embedded bulk iron are calculated by Equation 1:

$$E_d = E[Fe + A_2B_2O_7] - E[Fe] - E[A_2B_2O_7] \quad (1)$$

where 4 Fe atoms are removed in the Fe matrix, while A and B represent variable atomic elements and O represents oxygen. Note that positive (negative) dissolution energy is endothermic (exothermic).

The atomic models for first principle calculations are constructed as shown in Figure 1. Gas phase oxide clusters $A_2B_2O_7$, where A and B represents the atomic element and O represents oxygen, are constructed as such oxides are commonly observed in ODS alloys [14, 15]. 29 different gas phase oxide clusters, $A_2B_2O_7$, are constructed. The base structure of $A_2B_2O_7$, shown in Figure 1, is determined using the Basin-hopping algorithm where the ground state structures of $Y_2Hf_2O_7$ are explored and set as the base structure it is a well observed oxidized in ODS steel [15–17]. In particular, the following oxide clusters are considered: $Y_2Hf_2O_7$, $Y_2Ti_2O_7$, $Y_2Zr_2O_7$,

$Y_2Ni_2O_7$, $Sc_2Ti_2O_7$, $Nb_2Ti_2O_7$, Hf_4O_7 , $La_2Ti_2O_7$, Ti_4O_7 , $Ti_2Cr_2O_7$, Y_4O_7 , $Y_2Cr_2O_7$, $Y_2V_2O_7$, $Y_2W_2O_7$, Al_4O_7 , $La_2Hf_2O_7$, $La_2Zr_2O_7$, Ni_4O_7 , Si_4O_7 , $W_2Ti_2O_7$, $W_2Zr_2O_7$, $Y_2Ir_2O_7$, $Y_2Mo_2O_7$, $Y_2Re_2O_7$, $Y_2Rh_2O_7$, $Y_2Ru_2O_7$, $Y_2Ta_2O_7$, $Sc_2Hf_2O_7$, $Nb_2Hf_2O_7$. These oxide clusters are optimized using the Γ point where 15 Å vacuum is applied in all directions with 0.0 eV of smearing.

Oxide particles are experimentally observed to be embedded in the iron matrix [3, 18]. Therefore, a $3 \times 3 \times 3$ supercell of body center cubic (BCC) iron is constructed for embedding oxide clusters. In particular, a chunk consisting of 4 Fe atoms are removed from the $3 \times 3 \times 3$ supercell of BCC iron in order to create the vacancy site as shown in Figure 1. The constructed 29 oxides clusters are then embedded into the vacancy site of bulk iron.

Lattice optimization of oxide-embedded bulk iron is performed in order to find the optimized lattice constant. Once an optimized lattice is determined, further structural relaxation is performed in order to unveil the optimized atomic configurations. After lattice and structural optimization of oxide-embedded bulk iron is complete, 5% compression(expansion) is performed with taking 20 sample points where the equation of state is implemented in order to estimate the bulk modulus. Thus, the bulk modulus, lattice constant, and dissolution energies of oxides are calculated. The information resulting from the first principle calculations is then stored as a dataset for further data mining; the dataset is listed in Supporting Information [19].

III. COMPUTATIONAL RESULT

First principle calculations are performed in order to calculate the lattice constant (Å), bulk modulus (GPa), and dissolution energy (eV) of oxide clusters ($A_2B_2O_7$) in bulk iron. In general, ODS alloys are used in a high temperature environment with high strain such environments with exposure to shockwaves or high pressures. Within such extreme environments, one must consider minimalization of the thermal expansion of materials. A major indicator for resistance against thermal expansion is the bulk modulus as a high bulk modulus suppresses material expansion. Another important role of an ODS alloy in such an extreme environment is the pinning effect where point defects such as the alloying element or precipitation halts dislocation motion. The dissolution state of the oxide particles within the iron matrices also indicate whether the oxide particle can halt dislocation. If oxides particles and the iron matrix interact under endothermic matter, the oxides particles can be considered to be undissolved in the iron matrix. Undissolved oxide particles in iron matrices can be a point that halts the dislocation as a pinning effect. Thus, low solubility of oxides against an iron matrix plays an important role where the low soluble oxides act as point defects and halt the progression of dislocation.

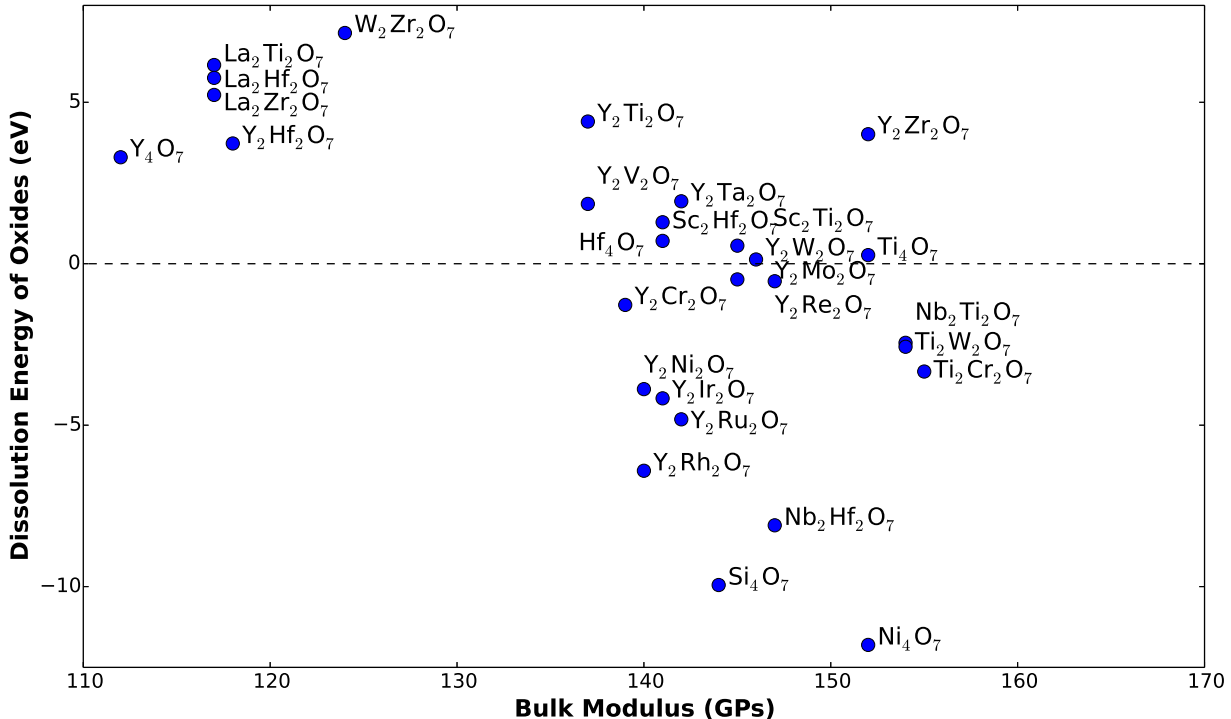


FIG. 2: Dissolution energy of oxide clusters ($A_2B_2O_7$) and bulk modulus (GPa) of oxide-embedded bulk iron.

Figure 2 plots the calculated bulk moduli and dissolution energies of the 29 cases of oxide-embedded bulk iron, where 0 is marked with a dotted line. For a high temperature environment with high strain, an oxide-embedded alloy with a high bulk modulus with endothermic (positive energy) is preferred in order to prevent thermal expansion and halt dislocation. In this sense, Figure 2 indicates that $Y_2Zr_2O_7$ and $Y_2Ti_2O_7$ have a positive dissolution energy with a high bulk modulus, making them good candidates as oxides for ODS alloys. This result shows good agreement with experimental reports where $Y_2Ti_2O_7$ is a commonly used oxide particles for ODS alloy [14, 20].

In addition, Figure 2 presents a correlation between the dissolution energy of oxides and the bulk modulus of oxide-embedded bulk iron. In particular, a low bulk modulus is achieved when the dissolution energy of the oxides is endothermic in bulk iron. On the other hand, a high bulk modulus is induced when the dissolution energy is exothermic and the dissolution energy is relatively close to 0 eV. This suggests that the dissolution energy of oxides could be a key descriptor representing the bulk modulus of oxide-embedded iron.

IV. DATA MINING METHOD

Calculated results from first principle calculations are stored as a dataset. In addition, corresponding informa-

tion such as electronegativity and electron affinity is also added into the dataset as element information often plays an important role to predict the material property. The constructed dataset is listed in Supporting Information. Machine learning is applied for predicting the dissolution energies of oxides in iron and the bulk moduli of oxide-embedded iron where cross-validation is used to measure the accuracy of the chosen descriptors.

Scikit-learn is used for the machine learning process [21]. In particular, support vector machine (SVM) and linear regression (LR) are implemented for predicting the dissolution energy and bulk modulus, respectively. Dissolution energy can be considered an indicator for the pinning effect and whether oxides are dissolved in exothermic or endothermic matter. Therefore, dissolution energy is classified as '0' and '1' which indicates endothermic and exothermic energy, respectively. Polynomial kernel is implemented for SVM. Bulk modulus is an indicator for resistance against thermal expansion; therefore, prediction of bulk modulus as a continuous value is performed. Ordinary least squares within linear regression is implemented for predicting bulk modulus.

Descriptors play a key role within machine learning where several physical factors are treated in multi dimensional space, resulting the prediction of physical phenomena [3]. Therefore, descriptors determining dissolution energy and bulk modulus are explored within the SVM and LR. Descriptors are chosen from a dataset which contains calculated results as well as information from

the periodic table. Descriptors are evaluated using cross-validation where an average score of 10 random train and test data sets are taken.

V. DATA MINING RESULT

A. Dissolution Energy

Prediction of dissolution energies of oxides in iron is performed using SVM. Dissolution energies are classified into binary groups '0' and '1' where 0 and 1 are exothermic and endothermic energies, respectively. Descriptors for determining the dissolution energy are explored using cross-validation and SVM where test and train dataset are randomly sorted to 10% and 90%, respectively. The score is evaluated by taking the average of 10 random test and train data sets. Cross-validation and SVM reveal that the following 4 descriptors are responsible for determining the dissolution energy of oxides ($A_2B_2O_7$) in iron: electron affinity of A, electron affinity of B, electronegativity of A, and electronegativity of B. The average score with 4 descriptors results in 93% accuracy with a highest score of 100 %.

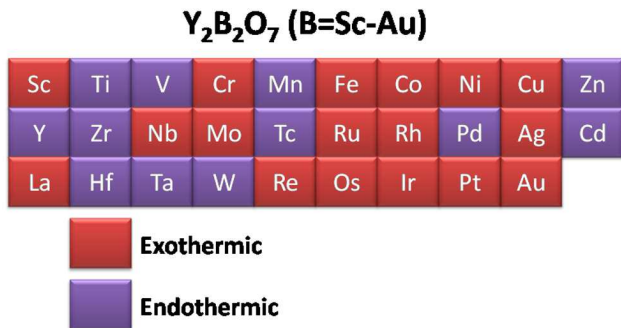


FIG. 3: Prediction of dissolution energy of oxides, $Y_2B_2O_7$ (B=Sc-Au), in iron. Red and blue indicate exothermic and endothermic states, respectively.

The prediction of dissolution energy is also performed using the trained SVM. In particular, the effect of element B in $A_2B_2O_7$ is considered. Yttrium is generally used as a base element for oxides in structural materials [14, 15, 20, 22]. However, it is not well understood which element would result in an exothermic or endothermic dissolution energy when an yttrium-based oxide cluster ($Y_2B_2O_7$) is embedded in iron. Therefore, a transition metal (Sc-Au) is used in place of B in $Y_2B_2O_7$ in order to determine if the dissolution energy will result in exothermic or endothermic energy using the trained SVM. Y and B (where B= Sc-Au) are transformed into descriptor variables electron affinity and electronegativity as the descriptors for predicting dissolution energy are found to be electron affinity of A, electron affinity of B, electronegativity of A, and electronegativity of B. The trained SVM

is then used to predict the dissolution energy which is defined as exothermic or endothermic. The predicted dissolution state of $Y_2B_2O_7$ (B=Sc-Au) in iron are shown in Figure 3. The dissolution state of oxides is viewed as an indicator of the pinning effect that halts dislocation. In light of this, the elements colored blue in Figure 3 are expected to possess such pinning effects when the element is used in place of B in $Y_2B_2O_7$. In addition, one can see that the left portion of elements in Figure 3 tends to exhibit endothermic reaction. Thus, the dissolution state of oxides can be understood when the electronegativity and the electron affinity of elements in the oxides are treated within a multidimensional space.

B. Bulk modulus

Prediction of bulk modulus of the oxide-embedded iron is performed using LR. Descriptors for predicting the direct bulk modulus of oxide-embedded iron is explored using LR and cross validation where the data set is sorted into 20% test data and 80% train data and the average score of 10 random test and train datasets are evaluated. Cross-validation reveals that the descriptors for predicting the oxide-embedded iron are as follows: dissolution energy of oxide in iron, density, lattice constant, and the difference in electronegativity of oxides ($A_2B_2O_7$). Figure 4 shows the true and predicted bulk moduli (GPa) of oxide-embedded bulk iron. Figure 4 demonstrates that the bulk modulus of oxide-embedded iron is well predicted with an average score of 84% accuracy with a highest score of 92% accuracy in cross validation.

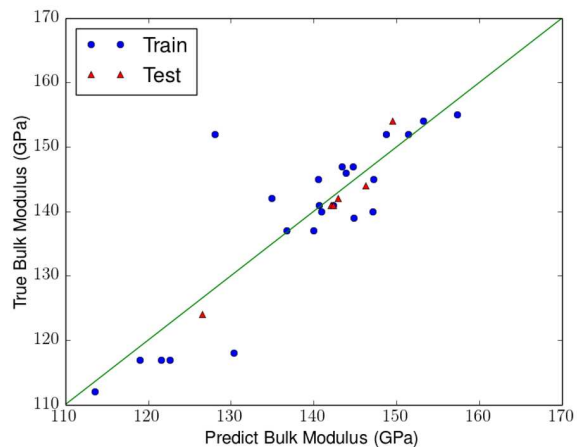


FIG. 4: True and predicted bulk modulus (GPa) of oxide-embedded bulk iron. Dataset is sorted into 20% test data and 80% train data.

The prediction of descriptor variables from a desired bulk modulus- essentially, the inverse problem- is performed using trained LR. In particular, every possible descriptor variable is generated and given to the trained

LR which returns the corresponding bulk modulus. The following sets of descriptor variables are considered: dissolution energy of oxides in iron(-5 eV to 5 eV with 10 cut), density(6.5 g/cm³ to 7.5 g/cm³ with 10 cut), lattice constant(3.05 Å to 3.10 Å with 10 cut), and difference in electronegativity of A and B in A₂B₂O₇(0.00 to 1.00 with 10 cut). Every combination of the listed variables is generated, resulting in a total of 10,000 combinations of descriptor variables. The 10,000 descriptor variables are given to trained LR which returns 10,000 corresponding bulk moduli; this can be viewed as generating big data using the trained LR. Once the big data is generated, it becomes possible to directly mine a desired bulk modulus and its corresponding descriptor variables. Descriptor variables satisfying a bulk modulus of 130 GPa, 140 GPa, 150 GPa, and 160 GPa are explored in the generated big data. Table I shows the corresponding descriptor variables satisfying the bulk modulus 130 GPa, 140 GPa, 150 GPa, and 160 GPa. Within 10,000 generated big data, three possible descriptor variables are screened out for 130 GPa ,140 GPa,and 150 GPa and one descriptor variable for satisfying 160 GPa. This indicates that the element in A₂B₂O₇ could potentially be predicted using a desired bulk modulus in this proposed approach. Thus, the bulk modulus of oxide-embedded iron can be predicted by using trained LR. Meanwhile, and big data can be constructed using trained LR where descriptor variables can be extracted using a desired bulk modulus from big data.

Bulk	Diss	Density	Lattice	Electro
130	2.77	7.38	3.09	0.00
130	3.88	6.83	3.09	1.00
130	5.00	6.94	3.08	0.11
140	1.66	7.83	3.07	0.00
140	2.77	6.83	3.07	1.00
140	5.00	7.50	3.08	0.55
150	1.66	6.83	3.06	1.00
150	2.77	6.61	3.05	0.00
150	3.88	7.50	3.06	0.55
160	-1.66	7.27	3.05	0.88

TABLE I: Bulk modulus with corresponding predicted descriptor variables . Bulk: Bulk modulus in GPa, Diss: Dissolution energy of oxides in iron in eV, Density: Density in g/cm³, Lattice: lattice constant in Å, Electro: difference in electronegativity of A and B in A₂B₂O₇.

VI. PHYSICAL MEANING

The physical origin behind the chosen descriptors is investigated on the basis of electronic structures of oxide-embedded bulk Fe. SVM reveals that the dissolution energy of oxides in iron can be predicted using the descriptors electronegativity and electron affinity of oxides. This suggests that the bond state between iron and the embedded oxide could play an important role. Four

oxides- Y₂Ni₂O₇, Y₂Ru₂O₇, Y₂Hf₂O₇, and Y₂Ti₂O₇- in iron are chosen for investigation as the dissolution energy of Y₂Ni₂O₇ and Y₂Ru₂O₇ in iron are exothermic while Y₂Hf₂O₇ and Y₂Ti₂O₇ in iron are endothermic. The projector density of state (PDOS) of the d-electrons of the metals and the p-electrons of oxygen in the chosen 4 oxides in iron are calculated and shown in Figure 5. Figure 5 (a) shows that the d-electrons of Ni overlap with the nearest d-electron of iron, indicating bonding between Fe and Ni atoms. This results in the exothermic dissolution energy of Y₂Ni₂O₇ in iron. In the same fashion, the d-electron of Ru also overlaps with the d-electron of iron as shown in Figure 5 (b). Thus, overlapping of iron and the metal atom within the oxide is observed in the electronic structure when the dissolution energy of the oxide is exothermic. On the other hand, the electronic structures of the oxides in iron behave differently when the dissolution energy is endothermic as seen in Figures 5 (c) and (d). Figure 5 (c) shows that there is no overlapping between the d-electron of iron and both of the d-electrons of the Hf and Y atoms. Similarly, neither of the d-electrons of Y and Ti overlap with iron as seen in Figure 5 (d). This results in endothermic dissolution energy. Thus, the electronic structures of the oxides in iron demonstrate that the overlapping of metal within the oxide and iron results in exothermic dissolution energy while endothermic dissolution energy is observed if the metal within the oxides and iron do not overlap.

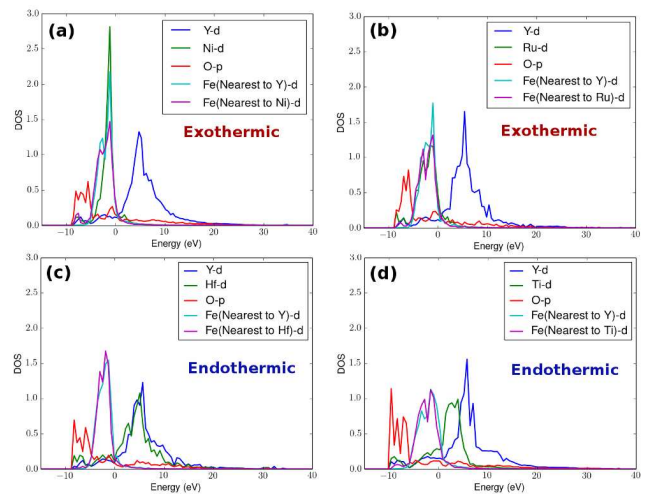


FIG. 5: Projector density of state (PDOS) of (a) Y₂Ni₂O₇, (b) Y₂Ru₂O₇, (c) Y₂Hf₂O₇, and (d) Y₂Ti₂O₇.

Other factors to consider are the electron affinity and electronegativity of A and B in A₂B₂O₇. Figure 5 demonstrates that the dissolution energy of oxides in iron can be understood by how metal in the oxides interact with nearby iron. The two physical factors governing the interaction between atoms are electron affinity and electronegativity. In fact, the following 4 properties- electron affinity of A, electron affinity of B, electronegativity of A, and electronegativity of B in A₂B₂O₇- are found

to be descriptors for predicting the dissolution energy of oxides. Individually implementing each descriptor does not provide the dissolution energy of the oxide; rather, the dissolution energy of the oxide is procured by combining these descriptors within a multidimensional space. Here, these 4 descriptors are plotted two dimensionally where electron affinity and electronegativity of the 29 oxides in the dataset are used. In particular, the sum of 'electron affinity of A and electron affinity of B' and the sum of 'electronegativity of A and electronegativity of B' in $A_2B_2O_7$ with the corresponding dissolution state 'endothermic' or 'exothermic' are plotted as shown in Figure 6. Figure 6 shows that endothermic dissolution energy can be expected when the sums of electron affinity and electronegativity of metal in the oxides are small while the sums of electron affinity and electronegativity are likely to result in an exothermic dissolution energy. The results reveal a correlation between 'electron affinity and electronegativity of the metal within the oxide' and the dissolution energy of the oxides in iron as seen in Figure 6. These physical variables can be considered to be responsible for determining the interaction between oxides and iron if each physical property is treated in a multidimensional space.

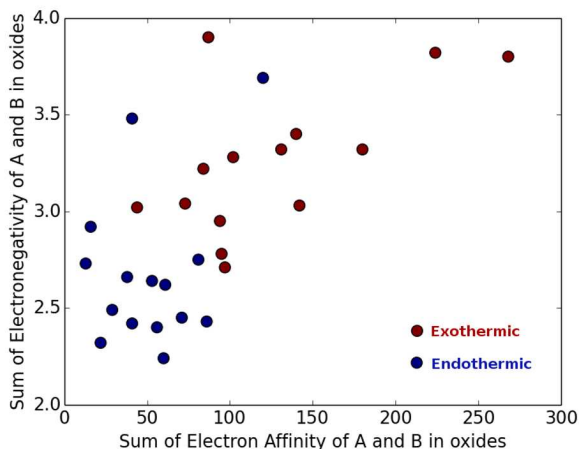


FIG. 6: Sum of 'electron affinity A and electron affinity B' and sum of 'electronegativity A and electronegativity B' in $A_2B_2O_7$ with corresponding dissolution state 'endothermic' or 'exothermic'

The bulk modulus of oxide-embedded iron can be predicted by using the following descriptors: dissolution energy of oxides in iron, density, lattice constant, and difference in electronegativity of oxides($A_2B_2O_7$) as shown in Figure 4. There is a correlation between the dissolution energy of the oxides within iron and the bulk modulus as seen in Figure 2. Figure 2 shows that the bulk modulus is small when the dissolution energy of the oxide is exothermic while a high bulk modulus is achieved when the dissolution energy of the oxide is endothermic. Figures 5 (a) and (b) show that bonding between the metal in the

oxide and the nearest iron occurs when the dissolution energy of the oxide is exothermic while Figures 5 (c) and (d) show that there is no bonding between metal in the oxide and the nearest iron if the dissolution energy of oxide is endothermic. One can also consider that a low bulk modulus is achieved when there is no bonding between oxides and Fe as such oxides behave as point defects while a high bulk modulus is a result of exothermic reactions as such oxides create bonds with surrounding Fe atoms. In addition, Figure 6 reveals that electronegativity and the electron affinities of A and B play an important role in determining the dissolution state of oxides. Thus, the bulk modulus of oxide-embedded iron can be understood by the dissolution energy of the oxides in iron and the difference in electronegativity of oxides($A_2B_2O_7$).

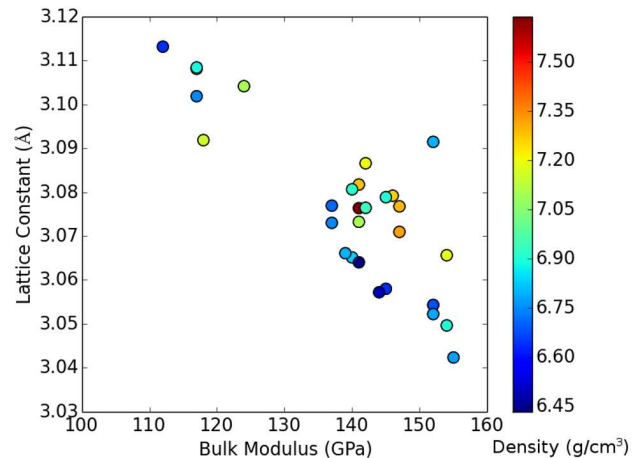


FIG. 7: Lattice constant (\AA) and bulk modulus (GPa) of oxide-embedded iron. Colorbar indicates the corresponding Density (g/cm^3).

The effect of density and the lattice constant against the bulk modulus is investigated as two of the descriptors for predicting the bulk modulus are density and lattice constant. The lattice constant and the bulk modulus with corresponding density is plotted and shown in Figure 7 where 29 oxides in the dataset are used. Figure 7 shows the linear relation between the lattice constant and the bulk modulus where a high bulk modulus is expected when the lattice constant is small while a small bulk modulus is predicted with a large lattice constant. In addition, density is added into this linear relation where various densities can exhibit within the same bulk modulus. For instance, a density from 6.4 (g/cm^3) to 7.5 (g/cm^3) would result in a bulk modulus of 140 GPa as shown in Figure 7. As a result, density gives a new dimension in Figure 7 where a variety of densities can be considered to achieve a specific bulk modulus.

Each descriptor involved in the prediction of the dissolution energy and bulk modulus has a physical correlation with each other, yet it is difficult to predict the dissolution energy and bulk modulus using a single descriptor. However, in principle, manipulating these de-

scriptors within a multidimensional space allows for the prediction of precise physical phenomena.

VII. CONCLUSION

In conclusion, oxide-embedded bulk iron is investigated in terms of combining first principle calculations and data mining. 29 different oxide clusters are embedded into a vacancy site of bulk iron. First principle calculations are performed to calculate the dissolution energy of the oxides and the bulk modulus of oxide-embedded iron where the calculated oxides with high bulk moduli and endothermic reactions with iron have good agreement with oxides used in high temperature structural materials. Data mining is utilized for the prediction of the dissolution energy of the oxides and the bulk modulus of oxide-embedded iron. Prediction of dissolution energy is performed using support vector machine where descriptors for dissolution energy are revealed to be electron affinity and electronegativity of the metals within the oxides. Prediction of the dissolution state of $Y_2B_2O_7$ ($B=Sc-Au$) is also achieved using trained SVM. The bulk modulus is predicted using linear regression where the lattice constant, dissolution energy, density, and difference in electronegativity are determined to be descriptors

and the inverse problem— deriving corresponding descriptors variables from a desired bulk modulus— is also addressed. The physical phenomena behind the descriptors are investigated where each individual descriptor for the dissolution energy and the bulk modulus correlate with each other. Although predicting the dissolution energy and the bulk modulus using a single descriptor is challenging, prediction of those properties can be achieved when the individual descriptors are combined simultaneously in a multidimensional space. By utilizing multidimensional space, the prediction of the dissolution energy and bulk modulus of oxide-embedded iron is achieved. Thus, if appropriate descriptors are determined and manipulated multidimensionally, the prediction of physical phenomena, in principle, can be achievable.

VIII. ACKNOWLEDGMENT

CPU time is funded by Materials research by Information Integration Initiative (MI²I) project of the Support Program for Starting Up Innovation Hub from Japan Science and Technology Agency (JST). Computational work is supported in part by Hokkaido university academic cloud, information initiative center, Hokkaido University, Sapporo, Japan.

-
- [1] A. Jain, S. P. Ong, G. Hautier, W. Chen, W. D. Richards, S. Dacek, S. Cholia, D. Gunter, D. Skinner, G. Ceder, *et al.*, *APL Mater.* **1**, 011002 (2013).
 - [2] A. Walsh, *Nat. Chem.* **7**, 274 (2015).
 - [3] K. Takahashi and Y. Tanaka, *Comput. Mater. Sci.* **112**, 364 (2016).
 - [4] A. Seko, A. Togo, H. Hayashi, K. Tsuda, L. Chaput, and I. Tanaka, *Phys. Rev. Lett.* **115**, 205901 (2015).
 - [5] L. M. Ghiringhelli, J. Vybiral, S. V. Levchenko, C. Draxl, and M. Scheffler, *Phys. Rev. Lett.* **114**, 105503 (2015).
 - [6] K. Takahashi and Y. Tanaka, *Dalton Trans.* **45**, 10497 (2016).
 - [7] A. Jain, K. A. Persson, and G. Ceder, *APL Mater.* **4**, 053102 (2016).
 - [8] A. Hirata, T. Fujita, Y. Wen, J. Schneibel, C. T. Liu, and M. Chen, *Nat. Mater.* **10**, 922 (2011).
 - [9] J. S. Benjamin, *Metall. Trans.* **1**, 2943 (1970).
 - [10] L. L. Hsiung, M. J. Fluss, S. J. Tumey, B. W. Choi, Y. Serruys, F. Willaime, and A. Kimura, *Phys. Rev. B* **82**, 184103 (2010).
 - [11] J. J. Mortensen, L. B. Hansen, and K. W. Jacobsen, *Phys. Rev. B* **71**, 035109 (2005).
 - [12] J. P. Perdew, K. Burke, and M. Ernzerhof, *Phys. Rev. Lett.* **77**, 3865 (1996).
 - [13] H. J. Monkhorst and J. D. Pack, *Phys. Rev. B* **13**, 5188 (1976).
 - [14] S. Yamashita, S. Ohtsuka, N. Akasaka, S. Ukai, and S. Ohnuki, *Philos. Mag. Lett.* **84**, 525 (2004).
 - [15] H. Oka, M. Watanabe, N. Hashimoto, S. Ohnuki, S. Yamashita, and S. Ohtsuka, *J. Nucl. Mater.* **442**, S164 (2013).
 - [16] D. J. Wales and H. A. Scheraga, *Science* **285**, 1368 (1999).
 - [17] K. Takahashi, H. Oka, and S. Ohnuki, *ACS Appl. Mater. Interfaces* **8**, 3725 (2016).
 - [18] C. Capdevila, G. Pimentel, M. Aranda, R. Remente-ria, K. Dawson, E. Urones-Garrote, G. Tatlock, and M. Miller, *JOM* **67**, 2208 (2015).
 - [19] See Supplemental Material at URL will be inserted by publisher for dataset used in this article..
 - [20] T. Okuda and M. Fujiwara, *J. Mater. Sci.* **14**, 1600 (1995).
 - [21] F. Pedregosa, G. Varoquaux, A. Gramfort, V. Michel, B. Thirion, O. Grisel, M. Blondel, P. Prettenhofer, R. Weiss, V. Dubourg, *et al.*, *J. Mach. Learn. Res.* **12**, 2825 (2011).
 - [22] M. Klimiankou, R. Lindau, and A. Möslang, *J. Cryst. Growth* **249**, 381 (2003).
 - [23] J. Enkovaara, C. Rostgaard, J. J. Mortensen, J. Chen, M. Dulak, L. Ferrighi, J. Gavnholt, C. Glinsvad, V. Haikola, H. Hansen, *et al.*, *J. Phys. Condens. Matter* **22**, 253202 (2010).
 - [24] J. Wadsworth and F. Froes, *JOM* **41**, 12 (1989).
 - [25] Y. Aoki, T. Namiki, T. Matsuda, K. Abe, H. Sugawara, and H. Sato, *Phys. Rev. B* **65**, 064446 (2002).